ELSEVIER

Cryogenics 39 (1999) 585–593

Cryogenics

Heat slug propagation in QUELL. Part I: Experimental setup and 1-fluid GANDALF analysis

R. Zanino [a,*], C. Marinucci [b,1]

[a] *Dipartimento di Energetica, Politecnico di Torino, 24, c. Duca degli Abruzzi, 10129 Torino, Italy*
[b] *EPFL, CRPP – Fusion Technology Div., CH-5232 Villigen PSI, Switzerland*

Received 17 March 1999; accepted 1 June 1999

Abstract

The experimental setup for heat slug propagation at zero current and field in the QUench Experiment on Long Length (QUELL) is described and re-evaluated. Eight inductively heated and four resistively heated runs are considered and analyzed with the 1-fluid GANDALF model, which assumes perfect coupling between bundle and hole helium in the two-channel cable-in-conduit conductor (CICC). Although adequate to predict the hydraulic response, the 1-fluid model exhibits an intrinsic limitation to accurately simulate the evolution of the conduit temperature at different sensor locations during heat slug propagation. In general it appears that the analysis of this type of slow transients requires a 2-fluid model, as considered in Part II of the present study.

Keywords: Cable-in-conduit conductors (A); Superconducting cables (A); Supercritical helium (B); Heat transfer (C); Fusion magnets (F)

Nomenclature

B	bundle region
C	constant for calibration of inductive heater
C_{st}	strand contribution to C
C_{jk}	jacket contribution to C
E_{cal}	calibrated energy deposited into conductor (J)
E_{nom}	nominal energy deposited into conductor (J)
G	mass flow rate (kg/s)
H	hole region
h_{eff}	effective heat transfer coefficient between bundle and hole helium
G_{in}	inlet mass flow rate (kg/s)
I_{hp}	current peak of inductive heater (A)
Int	integral (A^2 s), defined in Table 2
L_h	heater length (m)
p_{ref}	helium initial pressure (Pa)
Q_0	linear input power density (W/m)
R_h	heater resistance (W)
t	time (s)
t_{END}	end of transient (s)
T_B	helium temperature in cable bundle region (K)
T_H	helium temperature in central channel (hole) (K)
T_{in}	helium inlet temperature (K)
T_{jk}	temperature of titanium conduit (jacket) (K)
T_{max}	peak temperature of titanium conduit (K)
U	potential drop over heater resistance (V)
w	helium enthalpy (J/kg)
x	coordinate along conductor length (m)
x_S	sensor coordinate (m)

Greek

ΔG_{in}	difference between experimental and computed inlet mass flow (kg/s)
Δ_{kap}	effective thickness of the Kapton layer in the resistive heater
Δt	numerical time step (s)
$\Delta t\ (T_{max})$	time lag between experimental and computed maximum conduit temperature (s)
ΔT_{max}	difference between experimental and computed peak jacket temperature (K)
τ_Q	nominal heating time (ms)
ω	pulse frequency of inductive heater (Hz)
ρ	helium density (kg/m^3)

* Corresponding author. Tel. :+39-011-564-4490; fax :+39-011-564-4499.

E-mail addresses: zanino@polito.it (R. Zanino), claudio.marinucci@psi.ch. (C. Marinucci)

[1] Tel.: +41-56-310-3288; fax: +41-56-310-3729.

0011-2275/99/$ - see front matter
PII: S0011-2275(99)00074-0

1. Introduction

Heat slug propagation was used originally in the QUench Experiment on Long Length (QUELL) [1] for the assessment [2] of the thermal and hydraulic performance of the dual channel cable-in-conduit conductor (CICC), see Fig. 1, at zero current and field. The tests were performed in the SULTAN facility at Villigen PSI, Switzerland. An inductive heater (IH) and a resistive heater (RH) were used alternatively to deposit energy in the conductor, and ultimately in the flowing supercritical helium I. The resulting evolution of the temperature T_{jk} of the titanium conduit was measured at several sensors downstream of the heater (see Table 1), and used to estimate the energy deposited by the heater, and the average helium advection speed.

More recently, a renewed interest of a different kind has arisen on the question of heat slug propagation in dual channel CICC, in connection with the test program of the Toroidal Field Model Coil (TFMC) experiment [3,4], which is planned at the Forschungszentrum Karlsruhe, Germany. In the TFMC, an experimental evaluation of the superconductor critical properties will only be possible by heating the helium upstream of the joint, then letting it flow through the joint and downstream to the high field region in the conductor, where a quench could be initiated. If this strategy works or not, will depend on the delicate balance between (probably) degraded properties of joint vs. conductor, and magnetic field dependence of the current sharing temperature. A similar situation will occur in the test program of the inner and outer modules of the Central Solenoid Model Coil (CSMC) experiment [5,6], which is planned at JAERI Naka, Japan. Only an accurate code will be reliable for the prediction of such tests, and this further shows the need for the validation presented here as an essential ingredient for TFMC and CSMC predictive studies. Both TFMC and CSMC are part of the International Thermonuclear Experimental Reactor (ITER) program.

A preliminary analysis [7] of heat slug propagation in QUELL, restricted to a single experimental run, was performed in the past with the 1-fluid code GANDALF [8] and with the 2-fluid code MITHRANDIR [9], and the latter appeared to be more accurate. For dual channel CICC like QUELL, the 1-fluid model assumes perfect thermal and hydraulic coupling between the helium in the cable bundle region (B in the following) and in the central channel/hole (H in the following). On the contrary, finite (as opposed to zero) B/H coupling time and different thermodynamic conditions in the two regions are allowed by the 2-fluid approach. Both codes have also been validated subsequently against quench propagation data [10,11] from QUELL, and applied to the study of QUELL and ITER stability [12–14]. MITHRANDIR was also extended and validated against helium II thermal-hydraulic and quench data [15], and used to assess in principle the influence of B/H coupling on quench propagation in dual channel CICC [16].

Here we present a rather exhaustive study of a set of 12 heat slug propagation runs (E-02-05-001–E-02-05-012, briefly referred to in the following as $001,\ldots,012$) all performed in QUELL on 5 February 1997. The inductive heater (0.12 m long) was used for runs 001–008, while the resistive heater (2.3 m long) was used for runs 009–012, both being axially located near the center of the ~91 m long $(NbTi)_3Sn$ conductor (see Tables 1 and 2). In the inductive cases, the heater was on for $\tau_Q = 40$ ms, in the resistive ones for $\tau_Q = 300$ ms, in both cases depositing energies ranging over more than an order of magnitude (see Table 2). Therefore we can consider the present study as being representative of a very wide range of conditions. With respect to the work presented previously [7], also the geometrical and material input has been significantly updated, and a new calibration of the input energies has been performed (see below).

Part I of the present study is dedicated to a discussion of the experiment and of the input common to both codes, and to the presentation of the results of the 1-fluid GANDALF analysis. Part II, which comes in a companion paper [17], concentrates on the 2-fluid

Table 1
Location of inductive and resistive heaters and of CGR thermometers

Sensor	Location along conductor (m)			Heater	
TA1	0.140				
			40.929		RH
TA2	40.942				RH
TA3	42.910				RH
		42.960		IH	RH
		43.080		IH	RH
			43.229		RH
TA4	43.260				
TA5	44.817				
TA6	49.310				
TA7	53.802				
TA8	58.295				
TA9	90.821				

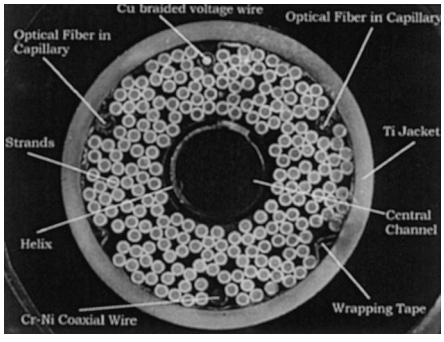

Fig. 1. Cross section of the QUELL conductor (courtesy of JAERI).

Table 2
Main features of the analyzed experimental runs E-02-05-XXX (zero current and magnetic field)

Run	I_{hp} (A)[a]	Int (A^2 s)[b]	ω (Hz)[c]	U (V)[d]	E_{nom} (J)[e]	E_{cal} (J)[f]	Q_0 (W/m)[g]
001[h]	170	576	952	–	131	85	17 708
002[h]	225	1013	952	–	231	185	38 542
003[h]	313	1955	952	–	446	339	70 625
004[h]	344	2365	952	–	539	424	88 333
005[h]	179	641	590	–	75	39	8125
006[h]	231	1067	590	–	125	92	19 167
007[h]	309	1907	590	–	223	188	39 167
008[h]	391	3050	590	–	357	303	63 125
009[i]	–	–	–	50	94	175	254
010[i]	–	–	–	120	540	633	917
011[i]	–	–	–	180	1215	1285	1862
012[i]	–	–	–	210	1654	1591	2306

[a] Current peak in heater.
[b] $\text{Int} = I_{hp}^2 \int \sin^2(2\pi\omega t)\,dt = I_{hp}^2 \tau_Q/2$.
[c] Pulse frequency.
[d] Potential drop over heater resistance R_h (nominal $R_h = 8\ \Omega$ @ 5 K).
[e] Nominal energy deposited into conductor (see text).
[f] Energy from calibration (see text).
[g] Linear input power density used in codes $Q_0 = E_{cal}/(L_h\ \tau_Q)$.
[h] Inductively heated run, heating time $\tau_Q = 40$ ms, heated length $L_h = 0.12$ m.
[i] Resistively heated run, heating time $\tau_Q = 300$ ms, heated length $L_h = 2.3$ m.

MITHRANDIR analysis. It also includes a study of the parametric effects of H friction factor, B/H coupling, varying insulation cross section, and a limited study of the numerical convergence of the code for heat slug transients.

2. Experimental setup and input parameters

In this Section we shall briefly review the setup of the experimental method for heat slug analysis in QUELL and discuss the input for the computational method.

2.1. Experimental setup and available diagnostics

The conductor used in the QUELL sample is made of $(NbTi)_3Sn$ strands developed for the ITER CSMC. The sample (Fig. 2), wound as a two-layer, non-inductive coil to minimize the coupling to the SULTAN coils, was

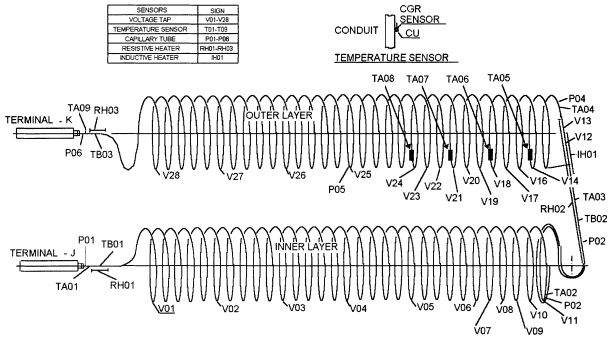

Fig. 2. Schematic diagram of sensor locations and types in the QUELL sample.

instrumented with conventional and novel quench detectors, i.e., 28 voltage taps, nine temperature sensors (CGR) and six pressure taps with cold pressure transmitters. The inductive heater was used to investigate heat slug propagation and stability, and the resistive heater for heat slug and quench propagation.

The main features of the experimental runs analyzed here have been summarized in Table 2. The values of I_{hp}, Int, ω and U come from the experimental log files. For the inductive runs, the nominal input energy was computed as $E_{nom} = C \times \text{Int}$. The constant C was estimated separately by the calorimetric method [18,19]. A first estimate [18], giving $C = C_{st} + C_{jk} \sim 0.01099 + 0.1059$, was done at 590 Hz and 40 ms, and should therefore be directly applicable to runs 005–008 (except the magnetic field is 7.7 T instead of 0 as here). Another measurement [19], giving $C = C_{st} + C_{jk} \sim 0.0226 + 0.2289$, was done previously at 1 kHz and 10 ms (and 9.65 T), but as such it is not directly applicable to runs 001–004. For these runs, taking into account that the induced eddy currents are proportional to ω^2, we apply a correction factor $(952/1000)^2$ to the experimental C. Notice that, as a byproduct of the previous estimates, *for all inductive runs only* $C_{st}/(C_{st} + C_{jk}) \sim 10\%$ *of the input energy goes directly into the strands*, while the remaining 90% goes into the jacket. For the resistive runs $E_{nom} = (U^2/R_h)\ \tau_Q$. Finally, the calibrated input energy E_{cal}, which is that actually used to determine the linear input power density needed by the codes, was computed as discussed in Section 2.2.

In the codes the heating pulses are simulated as square waves in space and time. This is essentially exact for the resistive cases, while for the inductive cases the square

time shape is still approximately true, considering that $2\pi\omega \gg 1/\tau_Q$ (see Table 2). The spatial shape of the inductive power is not exactly uniform [1,12], but this should not influence significantly the slow type of transients considered here.

The seven CGR thermometers TA2–TA8 used to measure the temperature of the Ti conduit (±10 mK accuracy between 5 and 20 K) are the major diagnostic tools, which we shall use for our validation (TA1 and TA9 are affected by significant conduction load from the current terminals [1] and will not be used here). From previous quench studies [1,11] it was also noticed that, because of the way the sensors are mounted on the conduit, a time delay of ~1–2 s is present in these signals, although this effect was not investigated in detail. Notice that (see Table 1) thermometer TA3 is nicely below the RH and as such it will be used for the calibration of the resistive heater model [17].

All experimental signals during heat slug runs in QUELL were collected with a 2 Hz resolution. Signals PI915 and PI916 will be used as inlet and outlet pressure, respectively (time dependent boundary conditions for the codes, together with prescribed constant inlet temperature $T_{in} = 5.05$ K for all runs). Signals PI915, TI 915 and dP903 will be used to deduce [20] the value of the experimental inlet mass flow G_{in}, which will be compared with the computed one (and also used for the calibration below). The pressure and temperature sensors PI915 and TI915 are located a few cm away from the sample inlet, and the differential pressure sensor dP903 is ~5 m upstream in the cryogenic system. The minor difference of helium conditions gives an estimated uncertainty [20] of the He density ρ of the order of a % ($G_{in} \sim \sqrt{\rho}$). PI915 and TI915 have been selected instead of signals PI903 and TI903, provided by sensors located near dP903 and used for online cryogenic diagnostics during the experiment, because the latter were not recorded by the data acquisition system.

2.2. Calibration of the energy input using thermometer signals

MITHRANDIR runs (not shown here) were initially performed with the nominal energy input E_{nom} from Table 2. They typically gave for all inductive cases a global overestimate of the conduit temperatures at the far downstream sensors (TA6–TA8). It was apparent that the system reacted in the simulation as if too much energy was being input. Therefore we decided to perform a new calibration of the energy input for both inductive and resistive runs, *based on the experimental traces of TA6–TA8*, and on other relevant experimental information (see below). The procedure is similar to that mentioned in [1,2], however a number of simplifying assumptions are involved in it, and we shall try and discuss them carefully in Appendix A.

Notice that, except at the lowest energies, for the inductive runs E_{cal} differs from E_{nom} by up to ~20%, for the resistive runs the discrepancy is even smaller. In both cases this is comparable with the measurement uncertainty [21].

Finally, and based on the previous discussion, we shall assume in the simulation of the inductive runs that 10% of the power is deposited in the strands, and the rest in the jacket, while in the simulation of the resistive runs the whole input goes to the jacket.

2.3. Definition of geometrical and material input parameters

We have to distinguish in general between three classes of input parameters: (1) geometrical parameters and material constants, (2) B/H coupling parameters (peculiar of MITHRANDIR), and (3) numerical parameters.

The major input parameters in the first class, common to both codes for the present study, are given in Table 3. These parameters can be easily translated into the standard GANDALF input parameters [11]. With respect to previous QUELL studies [7,10–12], two major differences are present in the input: (i) The jacket material is now Ti as in reality, instead of stainless steel, which was used previously in the simulations because Ti properties were not available to us at the time; (ii) It has been recognized that the insulation (with a rather complex structure by itself, see Part II [17]) is only present in the nonheated portion of the conductor. Consequently, the reference insulation cross section was chosen as AIN = 0 (see Part II for a study of the effects of different choices for AIN).

B/H coupling parameters specific of MITHRANDIR and numerical parameters for both codes will be discussed in Part II [17].

3. Results and discussion

Propagation of a heat slug is a relevant way to assess the thermal and hydraulic characteristics of a CICC with forced flow cooling, based on the observation of how the conductor reacts to the heat input by an external heater, in the absence of current and magnetic field. A temperature wave is induced and propagates both upstream and downstream of the heater location. In the meanwhile, the background helium flow is affected by the heat deposition during the initial transient, i.e., the heated helium is accelerated in both directions from the heater.

In this section we present and discuss results for four of the twelve experimental runs simulated with the

Table 3
Geometrical and material input parameters[a] for heat slug simulation in QUELL

Parameter	Symbol	Value	Units
Hydraulic length	XLENGT	90.961	m
Jacket outer diameter	DOUTJ	19.4	mm
Jacket inner diameter	DINJ	17.0	mm
Hole diameter	DHH	6.0	mm
Helix thickness	THICK	0.5	mm
Number of strands	NSTR	216	–
Strand diameter	DSTR	0.82	mm
Strand "pitch"	COSTETA	0.955	–
Cu–nonCu ratio	CURATIO	1.43	–
Strand "compression"	SCOMPR	5/6	–
Strand/jacket contact perimeter fraction	SJCONT	0.25	–
Insulation area	AIN	0.0	mm^2
Total sensor area	ASENSOR	4.909	mm^2
Total sensor perimeter	PSENSOR	15.71	mm
Copper RRR	RRR	260	–
Longitudinal strain[b]	EPSLON	-0.25×10^{-2}	–
SC critical temperature at zero field[b]	TC0M	17.67	K
SC upper critical field at zero temperature[b]	BC20M	30.15	T
SC material	$(NbTi)_3Sn$		
Jacket material	Ti		

[a] The corresponding GANDALF input parameters [9] are: AHEH $= 28.274\times10^{-6}$ m^2, AHEB $= 64.142\times10^{-6}$ m^2, ASC $= 49.154\times10^{-6}$ m^2, ACU $= 70.291\times10^{-6}$ m^2, ASS $= 68.612\times10^{-6}$ m^2, DHH $= 6.0000\times10^{-3}$ m, DHB $= 0.48106\times10^{-3}$ m, PHTC $= 463.70\times10^{-3}$ m, PHTJ $= 40.055\times10^{-3}$ m and PHTCJ $= 13.352\times10^{-3}$ m.
[b] The values of these parameters are taken from Ref. [1]. The critical current parameter C0 is not quoted because it is not used in these zero-current runs.

1-fluid code GANDALF (Figs. 3–6). This subset is sufficient to outline the most relevant results of the 1-fluid analysis, and is representative of the main features of all other runs. A detailed analysis of all runs will be presented in Part II [17].

In two of the four runs presented here the heat slug is generated by the inductive heater operated at 590 Hz (runs 005 and 008, Figs. 3 Figs. 4), in the other two by the resistive heater (runs 009 and 012, Figs. 5 Figs. 6). For each type of heater two limiting cases are compared: one at low energy (i.e., runs 005 and 009) and one at high energy (runs 008 and 012).

The variables used for the comparison between simulation and experiment are the jacket temperature T_{jk} at the location of the TA3–TA8 sensors, [2] and the helium mass flow at the conductor inlet, as functions of time.

3.1. General features of the experimental results

The jacket temperature traces at the sensors indicate that the heat slug profile broadens and correspondingly reduces its peak (i.e., diffuses along the conductor), while moving downstream.

The time profiles of T_{jk} are much narrower in the inductive than in the resistive runs. The effective heating time seen by the conductor in the resistive cases is much longer than τ_Q, [3] because heat is first conducted radially through the heater, and finally to the jacket. This, together with the longer heater length (2.3 vs. 0.12 m), explains the different width of the profiles in the inductive and resistive runs.

Concerning the inlet mass flow G_{in}, it can be seen that, depending on the energy deposited in the conductor, a strong reduction of G_{in} can be originated, sometimes even leading to flow reversal [4]. The time scale for this reduction is very different between inductive and resistive runs. In the former it is typically restricted to a very fast initial transient, while in the latter it can last for a

[2] Notice that, in the inductively heated runs, the simulated T_{jk} at the "heater sensors" TA3–4 reaches its maximum T_{max} on a time scale comparable or faster than the above mentioned delay in these thermometers, which is *not* included in the codes. Therefore, the comparison code/experiment at these sensors is not very reliable, because they react much slower than required in the inductive runs.

[3] For, e.g., run 012, the heater generates 2306 W/m (see Table 2). However, because of the internal heater structure, the maximum (computed) power density onto the jacket is about 60 W/m, reached after about 3 s, while it still is at ~30 W/m after 10 s, ~10 W/m after 20 s, and back to zero only for $t > 30$ s. Therefore, an effective heating time of ~10–20 s arises, to be compared with $\tau_Q = 300$ ms.

[4] In the inductively heated runs, only the simulations can reveal this effect, because the sampling rate for data acquisition is too slow to show the fast variation of G_{in}, which happens on the acoustic time scale.

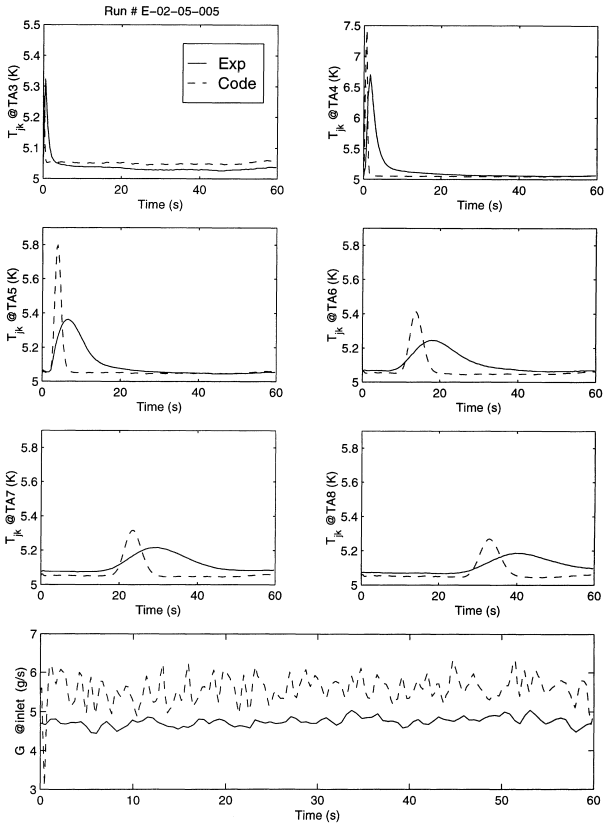

Fig. 3. Results of inductive run 005. Comparison between the time history of experimental (solid lines) and GANDALF (dashed lines) jacket temperature at sensors TA3–8 (top 6 subplots) and inlet mass flow (lowest subplot).

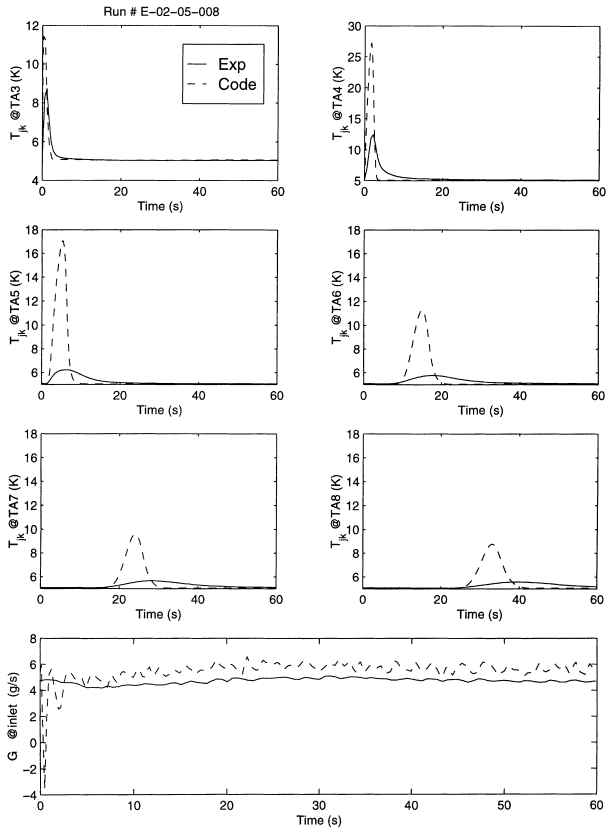

Fig. 4. Results of inductive run 008. Comparison between the time history of experimental (solid lines) and GANDALF (dashed lines) jacket temperature at sensors TA3–8 (top 6 subplots) and inlet mass flow (lowest subplot).

significant portion of the time required to return to steady state.

3.2. GANDALF results for inductively heated runs

The agreement between the simulated and the experimental peak jacket temperature T_{max} is acceptable only at low energy (Fig. 3). Because of heat conduction in the solids, the narrow profiles at the heater (40 ms width) diffuse while being convected along the conductor. Although the differences in T_{max} tend to smear in the downstream direction away from the heater ($\Delta T_{max}/T_{max} \sim 11\%$ at TA4, $\sim 8.1\%$ at TA5 and $\sim 1.6\%$ at TA8), the ratio between computed and experiment *jump* $(T_{max} - T_{in})$ is about constant. When a relatively high energy is deposited into the system (e.g., 303 J in run 008, see Fig. 4) $\Delta T_{max}/T_{max}$ becomes unacceptably large. In general, the time profiles of the simulated T_{jk} at the sensor locations are typically narrower than the experimental ones, so that the peak temperatures T_{max} are overestimated.

A second, somewhat independent observation is that the simulated T_{max} anticipates the experimental data at all TAs, and the time lag Δt (T_{max}) between experimental and computed T_{max} grows in the downstream direction (e.g., in run 005 Δt $(T_{max}) = 2.7$ s at TA5 and 8.0 s at TA8). This is due to the fact that the simulation overestimates the helium inlet mass flow, and therefore the mass flow everywhere in the conductor during the incompressible phases of the transient, at all times except during the initial phase. In run 005, e.g., $\Delta G_{in}/G_{in} \sim 15$–$20\%$ at steady state (Fig. 3). One likely cause for this overestimation is a too low friction factor assumed for the helium in the hole. [5] This parametric effect will be investigated with MITHRANDIR in Part II [17], since it is also present in the otherwise more accurate 2-fluid results.

Notice finally that the oscillations in the computed G_{in} are larger than in the experimental one. This is due to the fact that the computed mass flow is proportional to the measured $\sqrt{(\text{PI915-PI916})}$, which has a rather sig-

[5] The friction factor used for the helium in the bundle (f_B) and for the helium in the hole (f_H) are the same as in a previous quench study [11]. The Katheder correlation is used for f_B [22], while f_H is given by the usual correlation for smooth circular pipe, corrected by an artificial factor [2] FFCORH = 2.5, because of the presence of the helix.

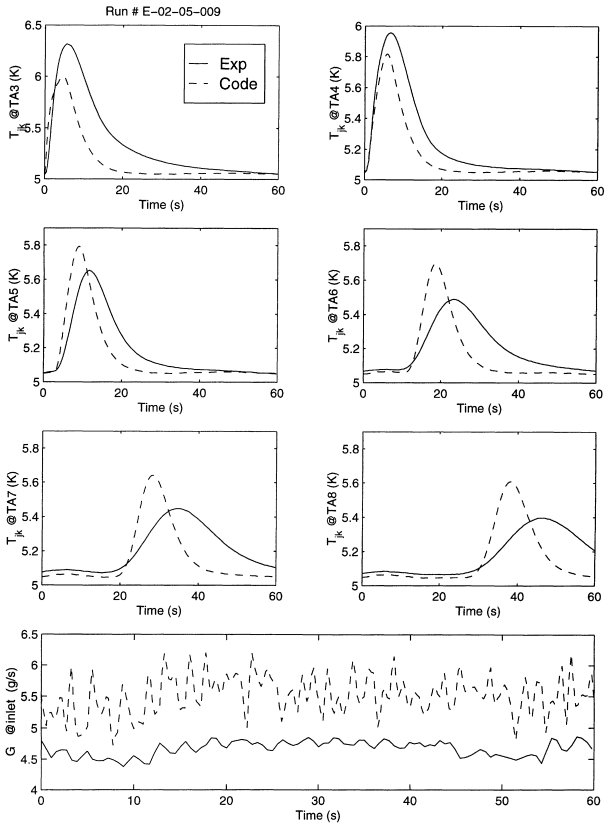

Fig. 5. Results of resistive run 009. Comparison between the time history of experimental (solid lines) and GANDALF (dashed lines) jacket temperature at sensors TA3–8 (top 6 subplots) and inlet mass flow (lowest subplot).

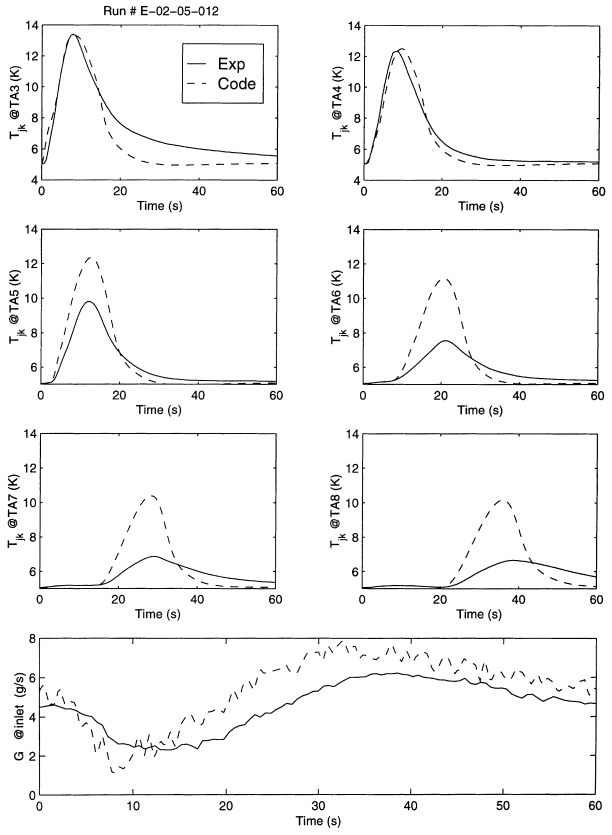

Fig. 6. Results of resistive run 012. Comparison between the time history of experimental (solid lines) and GANDALF (dashed lines) jacket temperature at sensors TA3–8 (top 6 subplots) and inlet mass flow (lowest subplot).

nificant oscillation, while the experimental inlet mass flow is proportional to the measured $\sqrt{(\mathrm{DP903})}$, which has a much smaller oscillation. This consideration applies to all runs considered here.

3.3. GANDALF results for resistively heated runs

A simplified model of the resistive heater (see Part II [17] for details) has been calibrated by adjusting the thickness Δ_{kap} of the Kapton layer in order to match the peak jacket temperature at TA3 in run 012. The optimized $\Delta_{\mathrm{kap}} = 2.1$ mm has then been used for all resistive runs.

The agreement of $T_{\max}$ is acceptable at all TA locations only in case of low input energy (in run 009, Fig. 5, $\Delta T_{\max}/T_{\max} < 5\%$), as was the case in the inductive runs. At high energy (run 012, Fig. 6) this agreement is good only at TA3, where it is enforced by the heater calibration, but it quickly deteriorates in the downstream direction away from the heater, with significant overestimation of $T_{\max}$ (e.g., $\Delta T_{\max}/T_{\max} \sim 25.9\%$ at TA5, and $\sim$52.4% at TA8).

At low energy, the simulation anticipates the experiment at all TAs. $\Delta t(T_{\max}) \sim 1$ s at TA3 and $\sim$9 s at TA8, again most likely because of the overestimation of G_{in} by $\sim$20% (run 009, Fig. 5). At high energy (run 012, Fig. 6), the simulated and experimental $T_{\max}$ are well synchronized not only at TA3, as imposed by the criterion used for the heater calibration, but also at the downstream sensors. This is due to the fact that the time average of the inlet mass flow is well reproduced for the first part of the transient. Qualitatively, the simulated G_{in} is in good agreement with the experiment for the whole transient, and correctly predicts the trend of the experimental flow: expansion of the helium slug for $0 < t < 15$ s, compression for $15 < t < 35$ s, and return to quasi-steady state conditions for $t > 45$ s.

4. Summary

The evolution of T_{jk} at the downstream sensors can be considered to be mainly affected by three effects: (1) *effective* time duration, and spatial length, of the heating pulse; (2) heat conduction in the solid components of the conductor, dominated by the conductivity of copper strands (jacket and strands are well thermally coupled by the helium, while direct contact plays a minor role);

(3) finite thermal coupling time between bundle and hole helium, flowing at different speeds.

The latter effect is the only one of the three to be intrinsically 2-fluid. A simple analysis [23], valid in the limit of $|T_B - T_H|/(T_B + T_H) \ll 1$, shows that although the helium heat conductivity is negligible (and therefore not included in the models) the combination of finite *radial* heat transfer coefficient h_{eff} between bundle and hole helium, and of velocity shear $\Delta V \equiv (V_H - V_B)$ between the two regions, leads to an effective helium heat conductivity *along the conductor*, which is proportional to $(\Delta V)^2/h_{eff}$. Since $h_{eff} \to \infty$ in the 1-fluid model, this effect cannot appear there.

As to the diffusion of the heat slug along the conductor, both effects (2) and (3) mentioned above will contribute, albeit to a different extent. Pure convection of the profile at the heater would obviously lead to unchanged profiles along the conductor.

In both inductively and resistively heated runs it was noticed that the 1-fluid GANDALF results systematically overestimate the experimental T_{jk} at the downstream sensors TA6–8. This is easily explained observing that the 1-fluid model does not include effect (3) above, and therefore typically underestimates the diffusion of the heat slug. Therefore, although adequate to predict the hydraulic response, the 1-fluid model exhibits an intrinsic limitation to accurately simulate the thermal evolution during a heat slug.

Notice, however, that the 1-fluid model was previously successfully validated for quench studies [11], and proved to be useful for stability studies [12,14], and this is not put in question here. Indeed, in a quench the induced helium flow is much stronger than in a heat slug experiment. This leads to higher h_{eff}, and therefore better thermal coupling between bundle and hole, thereby making the use of a 1-fluid approximation more justified [7].

Acknowledgements

The European Community Fusion Technology Program under contracts to R.Z. and C.M. has partially financially supported this work. We also wish to thank A. Anghel (CRPP), L. Bottura (CERN), P. Bruzzone (CRPP), L. Savoldi (POLITO) and Y. Takahashi (JAERI) for discussions, informations and help on the subject of this paper. A preliminary version of this report was presented at the Second TFMC Test Group Meeting at Forschungszentrum Karlsruhe, Germany, on 4 February 1999, and comments from several participants to the meeting are also gratefully acknowledged. Finally, we are thankful to one referee for several observations, which led to an improvement of the readability of the paper.

Appendix A. Computation of the calibrated energy input E_{cal}

Let us imagine to write down the total (B + H helium, stands, conduit) energy balance. We now integrate it in time from the beginning of the heat pulse to the end of the transient @ $t = t_{END}$ (when all variables are assumed to be back to their initial value), and in space from conductor inlet to the position $x = x_S$ of a generic sensor TAX (the same procedure is followed for each downstream sensor TA4–8). The $\partial/\partial t$ terms have to be integrated in time first, the $\partial/\partial x$ terms in space first, and the linear input power density Q_0 will give E_{cal}. The $\partial/\partial t$ contribution vanishes, since we integrate in time between $t = 0$ and $t = t_{END}$ and exact differential. We now assume that @ $x = x_S$ we are sufficiently downstream to ignore the conduction flux in the solids, so that the balance, under the further assumptions of negligible kinetic energy density with respect to internal energy density, and of same thermodynamic state of the helium in both B and H regions reduces to

$$E_{cal} = \int_0^{t_{END}} \left[Gw|_{x=x_S} - Gw|_{x=0} \right] dt, \tag{A.1}$$

where G is the total (B + H) mass flow and $w(p, T)$ the enthalpy.

In order to be able to estimate the right-hand side from experimental data only, we first make the assumption of incompressible flow with uniform and constant G (notice that the results show that this assumption is not verified in the highest energy cases). Then G can be estimated as the time average of the experimental inlet mass flow G_{in}, until pulse start (from pulse trigger signal). Second, in order to estimate the inlet enthalpy we use as reference pressure the time average of the inlet pressure until pulse start, and as reference temperature the time average of T *at the given sensor* until pulse start. Finally, in order to estimate the enthalpy at the sensor we use as reference pressure the typical average between inlet and outlet of the initial pressure, $p_{ref} = 5.55$ bar, and as reference temperature the measured $T(t)$ at the given sensor, assuming $T_B = T_H = T_{jk}$. Both the latter assumption and the neglect of conduction heat in solids require the sensor to be sufficiently downstream, so that we shall restrict our considerations to TA6–8. The last quantity to be determined in the right-hand side of (A.1) is t_{END}, and this was done by inspection of the traces TA6–8, choosing the time when the signal approximately returned to its initial value. Typically $t_{END} \sim 100$–120 s. Once the above procedure has been repeated for TA6–TA8, we obtain the values of E_{cal} in Table 2 by averaging over the results obtained for the three sensors (spread typically $\leqslant 10\%$).

References

[1] Anghel A, et al. The quench experiment on long length (QUELL). Final report 1997.

[2] Hamada K, et al. Thermal and hydraulic measurement in the ITER QUELL experiments. Adv Cryo Eng 1998;43;197–204.

[3] Salpietro E. ITER toroidal field model coil (TFMC) design and construction. Fus Technol 1998;34:797–801.

[4] Komarek P, Salpietro E. The test facility for the ITER TF model coil. Fus Eng Des 1998;41:213–21.

[5] Mitchell N, et al. ITER CS model coil project. In: ICEC16 Proceedings, 1997:763–766.

[6] Tsuji H, et al. ITER Central Solenoid Model Coil Test Program (1998). Presented at The 17th IAEA Fusion Energy Conference.

[7] Zanino R, Bottura L, Marinucci C. A comparison between 1 and 2-fluid simulations of the QUELL conductor. IEEE Trans Appl Supercond 1997;7:493–496.

[8] Bottura L. A numerical model for the simulation of quench in the ITER magnets. J. Comput. Phys. 1996;125:26–41.

[9] Zanino R, De Palo S, Bottura L. A two-fluid code for the thermohydraulic transient analysis of CICC superconducting magnets. J Fus Energy 1995;14:25–40.

[10] Zanino R, Bottura L, Marinucci C. Computer simulation of quench propogation in QUELL. Adv Cryo Eng 1998;43:181–8.

[11] Marinucci C, Bottura L, Vecsey G, Zanino R. The QUELL experiment as a validation tool for the numerical code GANDALF. Cryogenics 1998;38:467–77.

[12] DePalo S, Marinucci C, Zanino R. Stability estimate for CICC with cooling channel using one and two-fluid codes. Adv Cryo Eng 1998;43:333–9.

[13] Zanino R, Marinucci C, Savoldi L. Two-fluid analysis of the thermal-hydraulic stability of ITER CS and TF super-conductors. In: ICEC17 Proceedings, 1998:361–364.

[14] Marinucci C, Savoldi L, Zanino R. Stability analysis of the ITER TF and CS conductors using the code GANDALF. IEEE Trans Appl Supercond, to appear.

[15] Zanino R, Bottura L, Savoldi L, Rosso C. MITHRANDIR+: a two-channel model for thermal-hydraulic analysis of cable-in-conduit super-conductors cooled with helium I or II. Cryogenics 1998;38:525–31.

[16] Zanino R, Savoldi L, Tessarin F, Bottura L. Effects of bundle/hole coupling parameters in the two-fluid thermal-hydraulic analysis of quench propagation in two-channel cable-in-conduit conductors. IEEE Trans Appl Supercond, to appear.

[17] Zanino R, Marinucci C. Heat slug propagation in QUELL. Part II: 2-fluid MITHRANDIR analysis, Cryogenics, to appear.

[18] Koizumi N, Ito T. Calibration of inductive heating energy of QUELL conductor by calorimetric method. Report JASC-96-638 1996 (5 p.).

[19] Ito T, et al. Evaluation of inductive heating energy of Quench Experiment on Long Length (QUELL) conductor with the calorimetric method. In: ICEC16 Proceedings 1996:1301–1304.

[20] Anghel A. Private communication, 1998.

[21] Takahashi Y. Private communication, 1998.

[22] Katheder H. Optimum thermohydraulic operation regime for cable in Conduit Superconductors CICS. In: ICEC15 Proceedings 1994:595–598.

[23] Shaji A, Freidberg JP. In Ref. 1, pp. 128–130.